A high throughput study of both compositionally graded and homogeneous Fe–Pt thin films

Yuan Hong, Isabelle de Moraes, Gabriel Gomez Eslava, Stéphane Grenier, Edith Bellet-Amalric, Andre Dias, Marlio Bonfim, Laurent Ranno, Thibaut Devillers, Nora Dempsey

Available online at www.sciencedirect.com

jmr&t Journal of Materials Research and Technology

journal homepage: www.elsevier.com/locate/jmrt

Original Article

A high throughput study of both compositionally graded and homogeneous Fe–Pt thin films

Yuan Hong [a,*], Isabelle de Moraes [a], Gabriel Gomez Eslava [a], Stéphane Grenier [a], Edith Bellet-Amalric [b], Andre Dias [a], Marlio Bonfim [c], Laurent Ranno [a], Thibaut Devillers [a], Nora M. Dempsey [a,**]

[a] Univ. Grenoble Alpes, CNRS, Grenoble INP, Institut NEEL, 38000, Grenoble, France
[b] Univ. Grenoble Alpes, CEA, Grenoble INP, IRIG, PHELIQS, 38000, Grenoble, France
[c] DELT, Universidade Federal Do Paraná, Curitiba, Brazil

ARTICLE INFO

Article history:
Received 4 November 2021
Accepted 7 March 2022
Available online 12 March 2022

Keywords:
Permanent magnets
FePt films
Compositionally graded films
High throughput characterization

ABSTRACT

Compositionally graded Fe–Pt thin films were prepared on stationary 100 mm Si substrates by magnetron sputtering a base target of Fe on which a piece of Pt is asymmetrically positioned. Energy dispersive X-ray analysis was used to map the variation in film composition across the substrate, as a function of the size of the Pt piece. A scanning polar Magneto-Optical-Kerr-Effect system was used to probe the influence of composition and post-deposition annealing conditions (temperature and time) on coercivity. In this way, the maximum coercivity achievable for the sputtering system used could be established in a high throughput fashion. The evolution in coercivity with composition was correlated with the formation of $L1_0$ FePt and changes in its lattice parameters, as determined by scanning X-ray diffraction. High throughput coercivity mapping was then carried out on homogeneous Fe–Pt thin films of different compositions treated to different annealing conditions. This study serves as a step towards the integration of coercive FePt films into collectively fabricated devices.

1. Introduction

The functional magnetic properties of magnetic films depend on their crystallographic structure and microstructure (grain size, grain orientation, secondary and grain boundary phases …). These in turn depend on the films' chemical composition as well as the deposition and annealing conditions applied during film fabrication. Combinatorial thin film studies, based on the preparation and characterisation of compositionally graded films, are being used for the high-throughput screening and optimization of a range of functional materials [1–4], including hard magnetic films [5–7]. In a recent perspective, A. Ludwig [8] discussed the possibilities offered by combinatorial synthesis and high-throughput characterization in combination with computational methods to

* Corresponding author.
** Corresponding author.
E-mail addresses: yuan.hong@neel.cnrs.fr (Y. Hong), nora.dempsey@neel.cnrs.fr (N.M. Dempsey).
https://doi.org/10.1016/j.jmrt.2022.03.055

efficiently identify new materials in multi-dimensional search spaces, including ternary, quaternary and pentanary compounds. The author also commented that, although combinatory deposition methods for thin films and multilayers are well-established, further automatization of high throughput characterization methods is needed to accelerate materials discovery.

The $L1_0$ FePt phase of the Fe–Pt system has high magnetocrystalline anisotropy ($K_1 = 6$ MJ/m^3) and excellent chemical stability [9–11]. $L1_0$-based FePt thin films are extensively studied for use in several advanced magnetic recording techniques, including heat-assisted magnetic recording, exchange-coupled composites, graded media and bit patterned media as well as for micro-electromechanical systems (MEMS) applications [12]. Ludwig et al. [5] prepared Fe–Pt wedged multilayer thin films with a broad composition range and studied how coercivity and magnetisation varied as a function of composition and annealing conditions. The advantage of this combinatorial approach is that all compositions are treated to exactly the same set of annealing conditions, thus avoiding sample-to-sample variations which may occur when samples are prepared and annealed individually. The continuous composition gradient also allows to accurately determine the composition at which a transition occurs. However, the magnetic characterization step used was a bottleneck as it required samples to be diced for individual measurement in a high field magnetometer, and such measurements typically take some tens of minutes to perform.

Comparison of the results from that study and other literature shows that the optimum reported composition and annealing conditions for maximizing coercivity or anisotropy energy in $L1_0$ FePt based bulk and thin film samples vary from publication to publication [13–19]. In the case of composition, the reported optimum values varied by a few atomic percent and moved from the Fe-rich side [5,19,20] to the Pt-rich side [18] of the phase diagram. Thus, when one wants to fabricate coercive FePt films in a given deposition system for a given application, one is faced with the task of selecting the appropriate film composition and applying appropriate annealing conditions. In this work, we prepared compositionally graded Fe–Pt films and characterised them both magnetically and structurally in a high throughput fashion, so as to establish near-optimum composition and annealing conditions. We then used high throughput magnetic characterisation to optimise the composition and annealing conditions of homogeneous films, so that they can be used to fabricate high coercivity films over large surfaces, rendering them suitable for integration into collectively fabricated devices.

2. Experimental

Fe–Pt films were fabricated by magnetron sputtering (DP850, Alliance Concept) of an Fe target (99.9%, Goodfellow) of diameter 75 mm, partially covered by Pt foil (99.95%, Goodfellow), onto stationary substrates. In the main study, compositionally graded films were produced by asymmetrically positioning the piece of Pt foil on the Fe target and the composition gradient was varied by changing the size of the Pt piece: 25×25 mm^2 (target #1), 37.5×25 mm^2 (target #2) and 50×25 mm^2 (target #3), shown in Fig. 1. In a secondary study, compositionally homogeneous films were produced by symmetrically positioning pieces of Pt foil on the concentric track of the Fe base target where the sputtering rate is highest, and the composition was varied by changing the size and disposition of the Pt pieces (Fig. 2). Films were deposited at room temperature with a bias voltage of 100 V, sputtering power of 40 W and an argon flow of 20 sccm on thermally oxidised Si substrates of diameter 100 mm. The target–substrate gap was set at 50 mm. All films had the following architecture: Si/SiO_2 (100 nm)/Ta (10 nm)/Fe–Pt (x nm)/Ta (10 nm), with nominal thickness of $x = 100$ nm for the compositionally graded films and $x = 50$ nm for the homogeneous films. 1D line-scans or 2D maps of composition of as-deposited films were made using energy dispersive X-ray (EDX, Oxford Instruments) analysis (spot size ~ 1 μm) in a scanning electron microscope (SEM, ZEISS). The nominal accuracy of the estimated composition values is of the order of ±1–2 at.%. Film thicknesses were measured using a stylus profilometer (Dektak, Veeco). Post-deposition annealing was carried out on full substrates using a rapid thermal annealing furnace (RTA, Jipelec), while it was carried out on quarter wafers using a tube furnace. High throughput magnetic characterisation was performed using an in-house developed scanning polar Magneto-Optic Kerr effect (MOKE) system with an integrated coolant-free bi-polar pulsed magnetic field generator and a laser spot size of roughly 50 μm [21]. The maximum field strength applied at the film surface during a given loop measurement was 4 T, which is significantly higher than the maximum field values of 0.3 T [22] and 2.3 T [23] used in previous high throughput MOKE studies of hard magnetic films. The duration of individual field

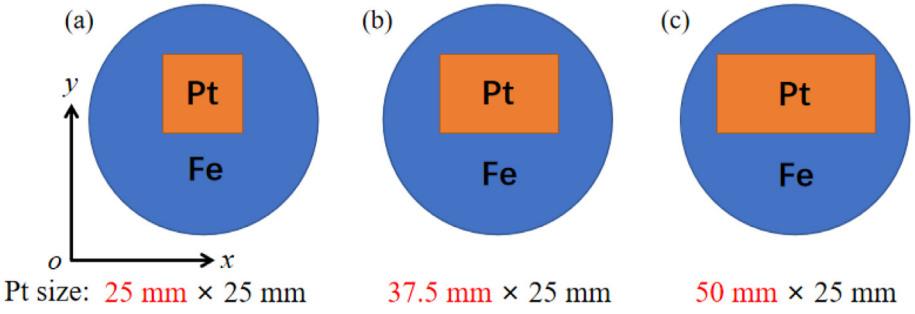

Fig. 1 – Schematic diagrams of the targets used to produce compositionally graded Fe–Pt films indicating the position and size of Pt foil on a base Fe target: (a) target #1, (b) target #2, (c) target #3.

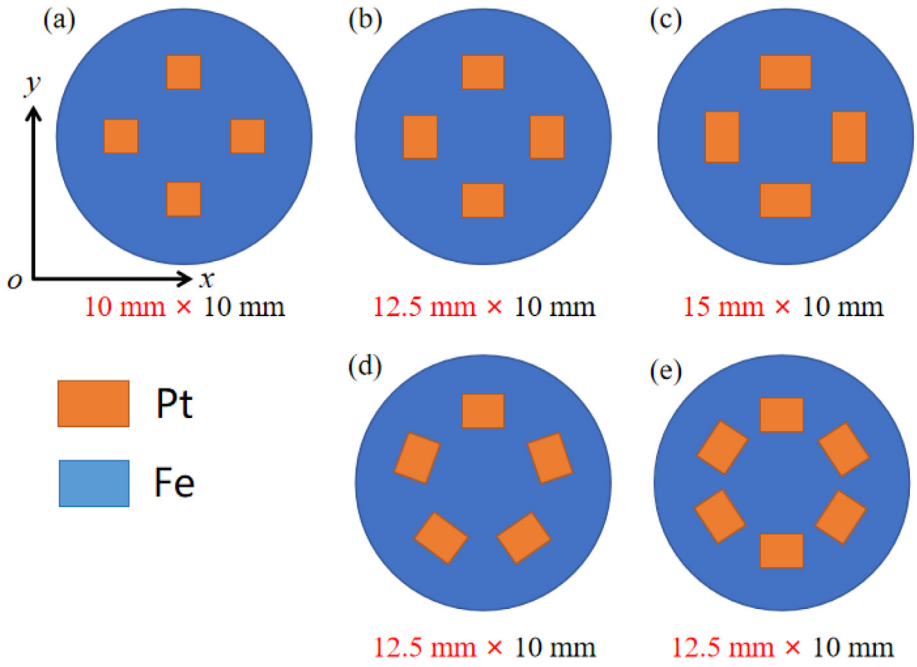

Fig. 2 – Schematic diagrams of the targets used to produce compositionally homogeneous FePt films indicating the position and size of Pt foils on a base Fe target: (a) target #4, (b) target #5, (c) target #6, (d) target #7, (e) target #8.

pulses is of the order of 16 μs, and the delay between positive and negative field pulses is roughly 10 ms. The coercivity of some reference sample pieces extracted from a compositionally graded film was measured using a SQUID-VSM (MPMS-3, Quantum Design). The evolution of crystal structure along the composition gradient was characterized in a high throughput fashion using scanning X-ray diffraction (XRD, Rigaku SmartLab) with Cu-K_α radiation.

3. Results and discussion

3.1. *Compositionally graded films*

One dimensional (1D) composition line-scans measured along the horizontal bi-sector (i.e., parallel to the y-direction) of films made from targets #1 - #3 are compared in Fig. 3. The equiatomic composition of $Fe_{50}Pt_{50}$ is found close to the centre of the film made with target #2, while it is positioned on the edges of the films made with the other two targets. Two dimensional (2D) EDX scans consisting of a matrix of 19 × 17 points (distance between each point = 5 mm, measuring time per point = 2 min) were made to probe for composition variations in both the x and y directions. Such a measurement takes roughly 12 h to perform. 2D composition maps of the films made using targets #2 and # 3 are compared in Fig. 4. The same colour scale bar is used in both figures, to emphasize the difference in composition spread. The observed variations in composition in the x-direction, which gives a somewhat wavy shape to the iso-composition lines, is attributed to slightly asymmetric positioning of the Pt piece on the Fe base target and/or to inhomogeneities of the plasma inside the sputtering machine. Such variations are not picked up in the 1D vertical scans, thus the interest in 2D scans. Having the expected optimum composition for the formation of $L1_0$ FePt close to the centre of the film allows the study of structural and magnetic

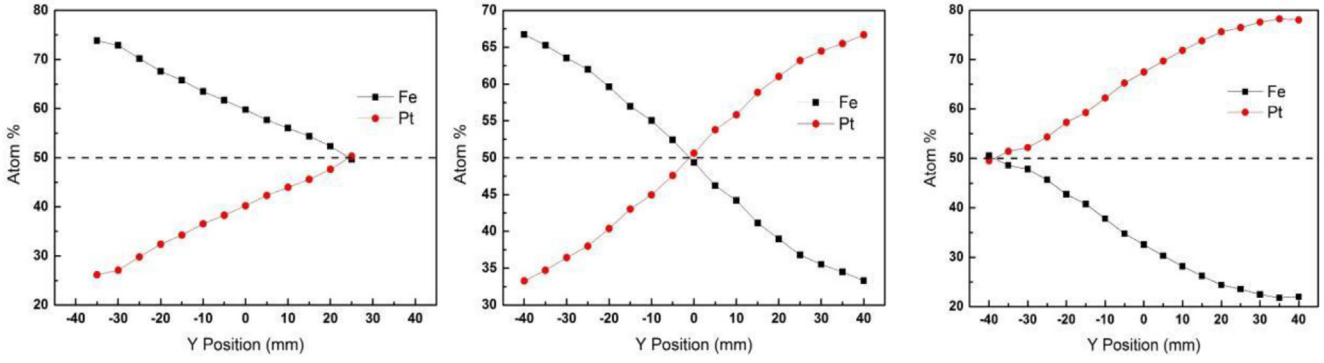

Fig. 3 – 1D EDX line scans of Fe and Pt content measured along the horizontal bi-sector (i.e., parallel to the y-axis) of samples fabricated using targets (a) #1, (b) #2 and (c) #3.

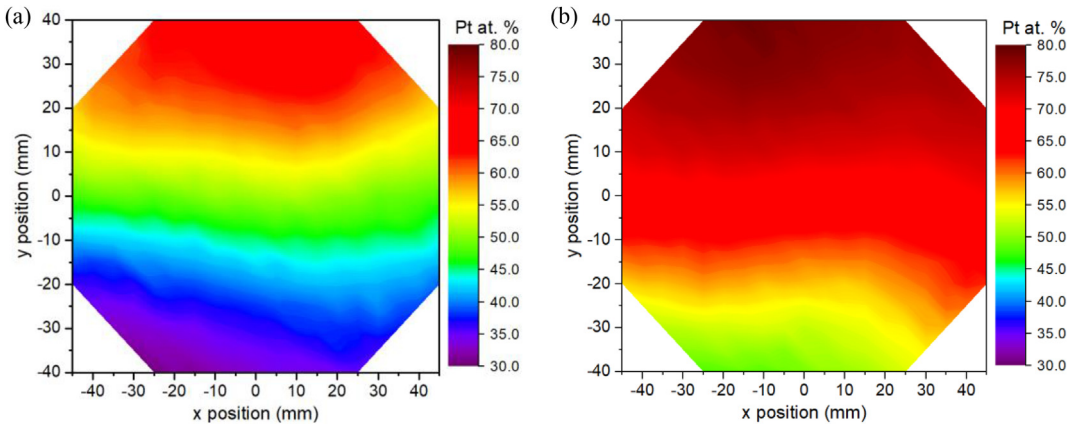

Fig. 4 – 2D EDX maps of Pt content measured over full wafers of films made using (a) target # 2 and (b) target # 3.

properties of films deposited under exactly the same conditions, in a composition range which is sure to include the optimum composition for a given annealing treatment. We thus identified target #2 as the most suitable target and all results reported on compositionally graded films hereafter concern films made from this target. The atomic composition of each element spans roughly 33–67% across the 100 mm substrate, which is a little narrower than the composition span of 25–75% reported by Ludwig et al. [5] for compositionally graded Fe–Pt films deposited on 150 mm substrates. A difference in the shape of the composition variations achieved (non-linear here vs. linear in the study of Ludwig et al. [5]) may be attributed to differences in the sputtering systems and the fabrication protocols used (Ludwig et al. deposited alternating opposing wedges of Fe and Pt).

To measure the variation in film thickness across the substrate for films made using target #2, a film was deposited onto a pre-patterned layer of resin. Post-deposition lift-off was then performed to produce a regular array of Fe–Pt islands with in-plane dimensions of 100 × 100 μm^2 and a mechanical stylus was used to measure the thickness of the micro-islands. A map of film thickness as a function of position on the wafer is shown in the supplementary materials file (S1). The maximum measured thickness corresponds to the nominal film thickness of 100 nm, and the region with this thickness is centred in the Pt-rich part of the film. The fact that this is off-centre with respect to the substrate is attributed to the higher argon sputtering yield of Pt compared to Fe [24]. The film thickness drops by roughly 30% on the Pt-rich upper edge of the film and 50% on the Fe-rich lower edge.

A set of compositionally graded Fe–Pt films prepared under identical conditions using target #2 were then annealed under different conditions and scanning high field MOKE was used for high throughput magnetic characterization. The first set of samples were annealed for 30 min at 500, 600 and 700 °C. Note that EDX mapping of the film annealed at the highest temperature of 700 °C (supplementary materials file S2) shows that annealing did not lead to any significant change in composition variation. Maps of MOKE loops of these samples are compared in Fig. 5. All three MOKE maps reveal the same overall trend, with coercivity increasing from practically zero in the Fe-rich bottom part of the wafer to a maximum value above the mid-point of the wafer followed by a reduction in the Pt-rich top of the wafer. Coercivity is a signature of the presence of the $L1_0$ FePt phase as neither $FePt_3$ nor Fe_3Pt phases have significant values of magnetocrystalline anisotropy. The variations in coercivity values seen in the MOKE maps are attributed to a combination of a number of factors. Firstly, the fact that the optimum annealing conditions for the ordering of the $L1_0$ phase depends on composition, as clearly demonstrated in calorimetry studies of Fe–Pt films [14] and in-situ neutron diffraction studies of ball milled Fe-Pt [9]. Secondly, the fact that coercivity is an extrinsic property that depends on microstructure (grain size, defects …), which can be expected to vary with composition and annealing conditions, even in single phase samples. Thirdly, intimate mixing of the high anisotropy $L1_0$ phase with soft magnetic $FePt_3$ or Fe_3Pt phases could lead to a drop in coercivity due to exchange and/or dipolar interactions between the phases. Finally, intimate mixing of the high anisotropy $L1_0$ phase with non-magnetic Fe-rich or Pt-rich phases could also modify coercivity through a modification in the microstructure.

The surface area over which relatively high coercivity values (>1T) are found is somewhat larger in the film annealed at the intermediate temperature of 600 °C, and the maximum value of coercivity measured in this film was roughly 1.6T. The highest values of coercivity (1.7–1.8 T) were found in the film annealed at 700 °C (positions identified by the red boxes in Fig. 5c). The fact that maximum coercivity is found on the edge of the film may be attributed to the observed drop in film thickness at the edge of the film. The 30% drop in film thickness at the Pt-rich film edge is thought to be too small to modify $L1_0$ ordering kinetics [14]. However, it may be enough to lead to an increase in coercivity through a reduction in grain size (see further discussion about this below). A zoom-in of some sample MOKE loops measured on the film annealed at 600 °C, at the regions identified by red boxes in Fig. 5b, are shown in Fig. 5d.

A side-by-side comparison of the EDX map of an as-deposited film made using target #2, and a map of coercivity values extracted from the MOKE loops of the film annealed at 600 °C for 30 min (shown in Fig. 5b), is made in Fig. 6. The coercivity is given by the averaged applied field value when the MOKE signal crosses through zero in the downward and

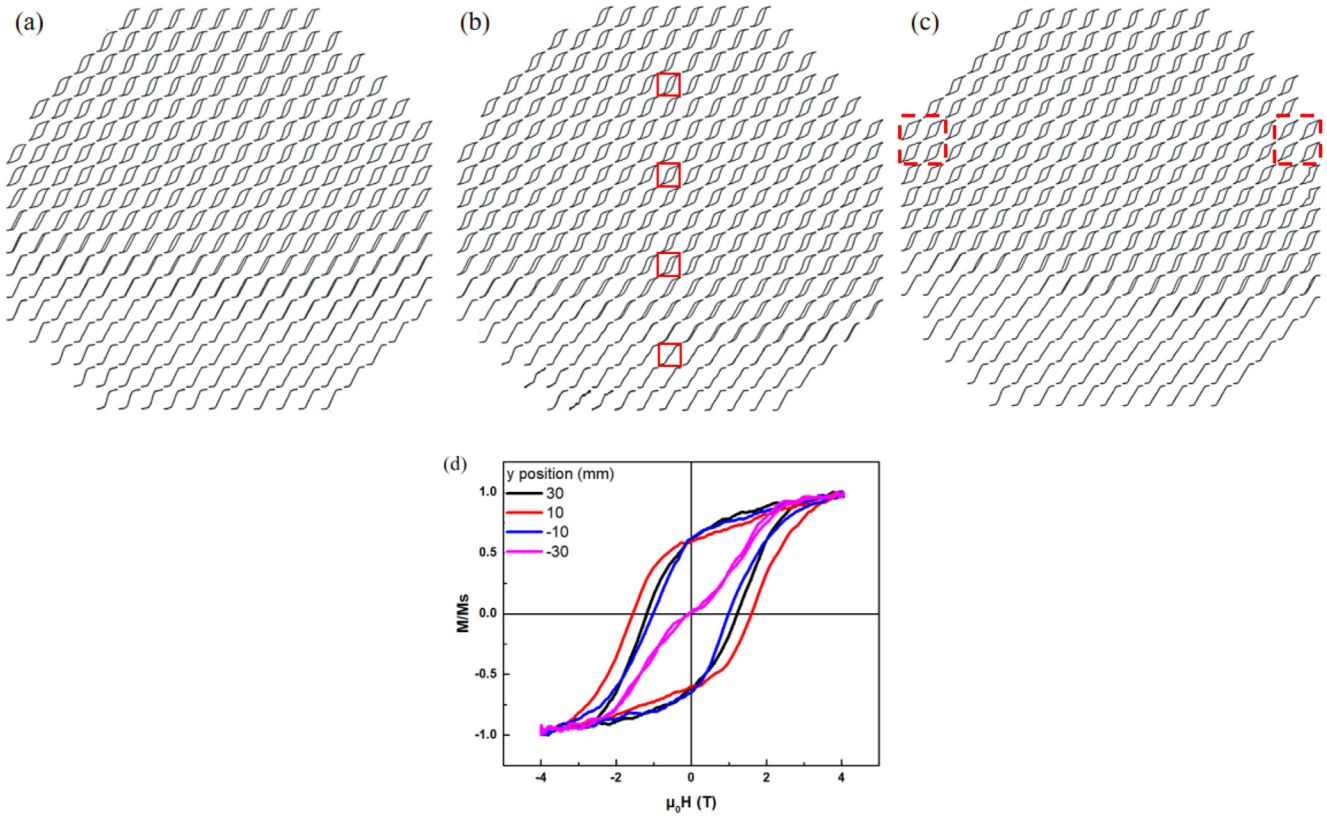

Fig. 5 – 2D Scanning polar MOKE maps of wafers, made from target #2, annealed at (a) 500 °C, (b) 600 °C and (c) 700 °C for 30 min (maximum applied field = 4 T; MOKE intensity values are normalised), (d) Enlarged typical MOKE loops from Fig. 5b at the regions identified by red boxes. (For interpretation of the references to colour in this figure legend, the reader is referred to the Web version of this article.)

upward branches of the loop. The horizontal variations in coercivity can clearly be associated with horizontal variations in composition. Coercivity is plotted as a function of Pt content, measured over the entire wafer, in Fig. 6c. Coercivity is seen to emerge at around 37.5 at.% Pt, peak at 1.6 T in the range 55–60 at.% Pt and then drop to just under 1 T at the max Pt content (~67.5 at.%). The spread in coercivity values seen for a given composition, which reaches 10% of the peak value, may reflect local variations in microstructure and film thickness. TEM imaging of the samples identified by the red boxes in Fig. 5b (supplementary materials file S3) reveals that these Fe–Pt films are between 1 and 2 grains deep. Thus a reduction in film thickness by 30% at the Pt-rich edges leads to a significant reduction in grain size, which could explain the observed increase in coercivity values at the film edges, for a certain composition range. We recall here that the aim of the present study is to identify the optimum nominal composition and annealing conditions for a given sputtering system to produce coercive FePt for subsequent integration into devices, rather than a fundamental study of the influence of composition variations on the coercivity achieved.

Phase formation and the degree of order depends on both the temperature and time of annealing and maps of MOKE loops of samples annealed at 600 °C for durations of 1, 10 and 30 min are compared in Fig. 7. The area of the zone showing high coercivity is found to increase with increasing annealing time.

To relate the observed changes in magnetic properties with variations in the crystallographic structure, X-ray analysis was carried out. An XRD waterfall pattern measured along a vertical section of the film annealed at 600 °C for 30 min, identified by a blue rectangle in Fig. 7c, is shown in Fig. 8. The distance between each measurement point is 2.5 mm while the X-ray beam spot is roughly 2–3 mm, allowing us to probe changes in crystallographic phases in an almost continuous fashion. The experimental data set is overlaid with the diffraction patterns of chemically ordered $L1_2$-$FePt_3$, $L1_0$-FePt and $L1_2$-Fe_3Pt, taken from ICSD reference cards 04-017-4976, 03-065-9121 and 04-001-3171, respectively. Peak indexation is the same for all three phases, with the $L1_0$ phase having additional peaks due to its tetragonal nature. The Fe–Pt diffraction peaks shift from higher to lower angle as we move up from the lower end of the wafer, indicating an expansion in lattice volume with increasing Pt content, since the metallic radius of Pt (138.5 pm) is much larger than that of Fe (126 pm). The experimental peaks at the Fe-rich end of the film are at a higher angle than those expected for ordered Fe_3Pt, as are the peaks of disordered Fe_3Pt [25]. This, together with the fact that only fundamental peaks ((111), (200) and (202)) are clearly identified, indicates the presence of disordered and/or off-stoichiometric $Fe_{3+x}Pt_{1-x}$ in this region of the film. A striking feature of this graph is the splitting of certain peaks ((200)/(002), (220)/(202), (311)/(113)), starting at around −25 mm on the y-axis, which can be clearly associated with

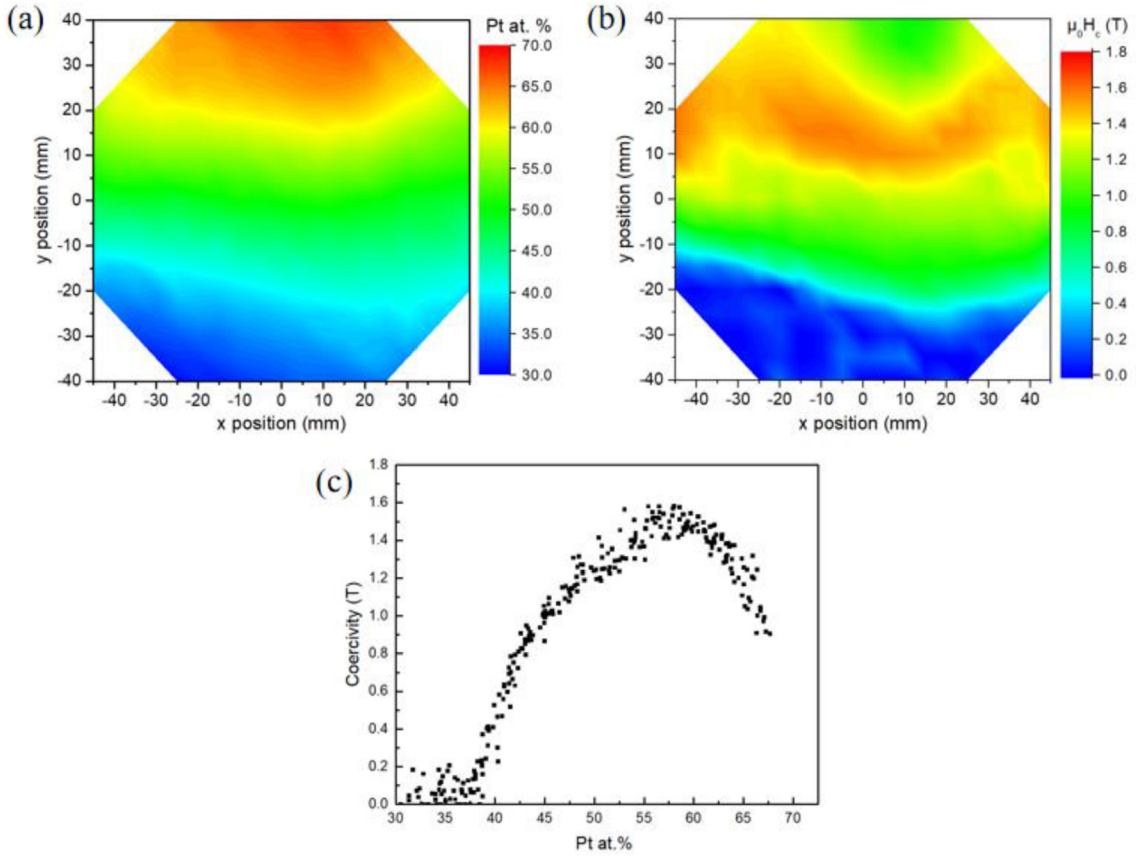

Fig. 6 – Comparison of (a) the Pt content EDX map of an as-deposited film made using target #2, and (b) a coercivity map extracted from MOKE loops measured on such a film annealed at 600 °C for 30 min (see Fig. 5b); (c) plot of coercivity as a function of Pt content, measured over the entire wafer.

the formation of the tetragonally distorted $L1_0$ FePt phase, with the degree of distortion increasing with Pt content. At the Pt-rich end of the film, the 2θ positions of most reflections are closer to those of $L1_0$ FePt than $FePt_3$, though lower angle shoulders indicate the presence of a Pt-rich phase. This is clearly seen in Fig. 9, which zooms in on the (111) diffraction peaks. The high relative intensity of the (111) and (222) peaks, compared to the expected intensities for an isotropic film is indicative of (111) fibre texture. Such a texture has often been reported for $L1_0$ FePt films. This apparent texture is sharpest in the upper Pt-rich part of the film and may explain the absence of certain peaks in these parallel beam X-ray diffraction scans. The unlabeled diffraction peak at 2θ ~ 28° is attributed to the presence of Ta_2O_5 (ICSD 00-025-0922), owing to surface oxidation of the Ta capping layer.

The *a* and *c* lattice parameters, estimated according to the angular position of the (200) and (001) peaks, respectively, are shown as a function of Pt content in Fig. 10, and compared with the values of $L1_0$ FePt, ordered and disordered Fe_3Pt and $FePt_3$. Distinct *a* and *c* parameters emerge above 35 at.% Pt,

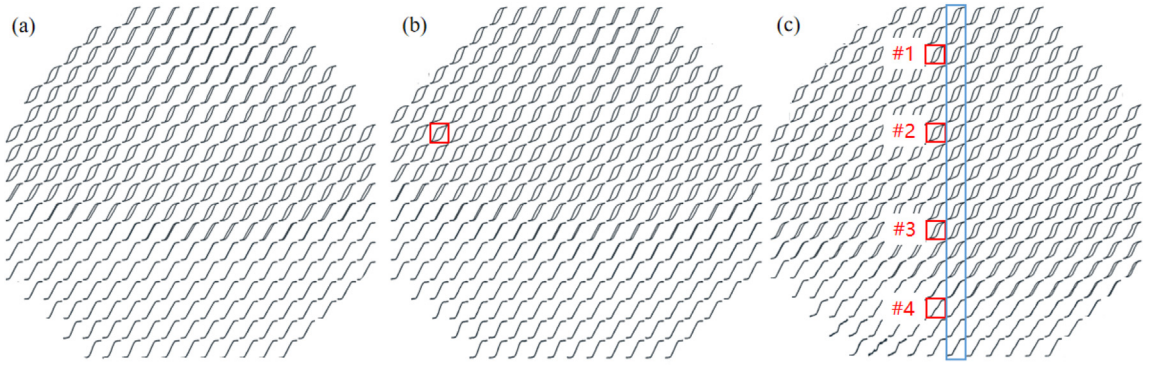

Fig. 7 – 2D Scanning polar MOKE maps of wafers, made from target #2, annealed at 600 °C for (a) 1 min, (b) 10 min (c) 30 min. Reference samples at the positions #1 to #4 were diced out of the wafer to make SQUID-VSM measurements.

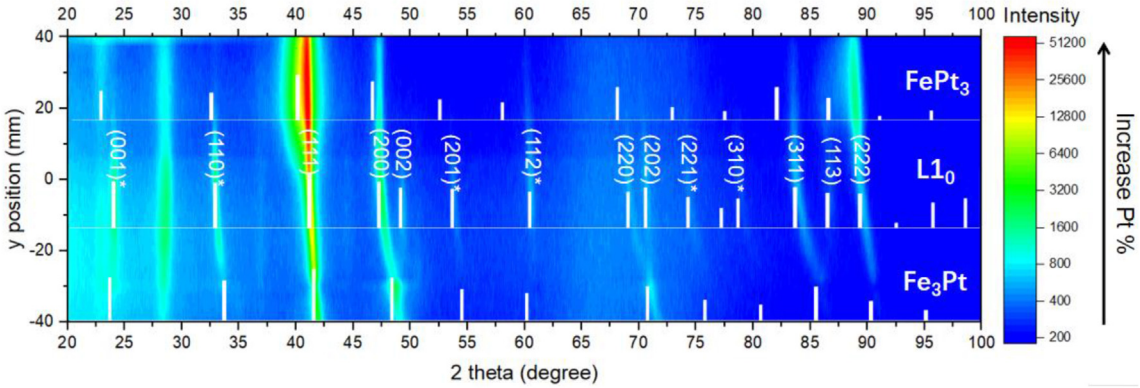

Fig. 8 – An XRD waterfall pattern, measured along the vertical section of the film annealed at 600 °C for 30 min, identified by the blue rectangle in Fig. 7c. The experimental data set is overlaid with the diffraction patterns of chemically ordered $L1_2$-$FePt_3$, $L1_0$-FePt and $L1_2$-Fe_3Pt, taken from ICSD reference cards 04-017-4976, 03-065-9121 and 04-001-3171, respectively. (For interpretation of the references to colour in this figure legend, the reader is referred to the Web version of this article.)

with the *c* value practically reaching that of $L1_0$ FePt above 37.5 at.% Pt, accounting for the emergence of coercivity at this composition. The *a* parameter steadily grows until reaching the value of the $L1_0$ phase at the composition where coercivity is maximum. The lattice parameter of cubic $Fe_{1+x}Pt_{3-x}$, labelled a*, emerges at about 57.5 at.% Pt and then steadily grows with increasing Pt content, indicating improved order with increasing Pt content. Intimate mixing of the high anisotropy $L1_0$ phase with non-magnetic Pt-rich phase could explain why the highest coercivity values are measured for a Pt content in the range 55–60 at.%. The presence of a non-magnetic secondary phase may increase coercivity by modifying the microstructure (e.g. weakening exchange interactions between grains of the $L1_0$ phase separated by the non-magnetic phase, pinning at inclusions of the non-magnetic phase …). Establishing the actual coercivity mechanism at play is beyond the scope of the present paper.

To recap the complementary nature of high throughput characterisation performed on compositionally graded Fe–Pt films, in Fig. 11 we replot select sections of XRD patterns together with the film composition, MOKE loops and coercivity values, plotted as a function of position along the vertical section of the film annealed at 600 °C for 30 min, identified by a blue rectangular box in Fig. 7c. The evolution in the film's coercivity with composition can clearly be correlated with the concomitant evolution in the crystallographic structure, and this compilation of graphs showcases the benefit of high throughput characterisation for screening the properties of compositionally graded hard magnetic films. The emergence of coercivity from the Fe-rich side coincides with the beginning of tetragonal distortion, at the position −25 mm, which has a nominal composition of around 36 at.% Pt. This is in good agreement with what was observed by Ludwig et al. [5] for compositionally graded Fe–Pt films annealed at 500 and

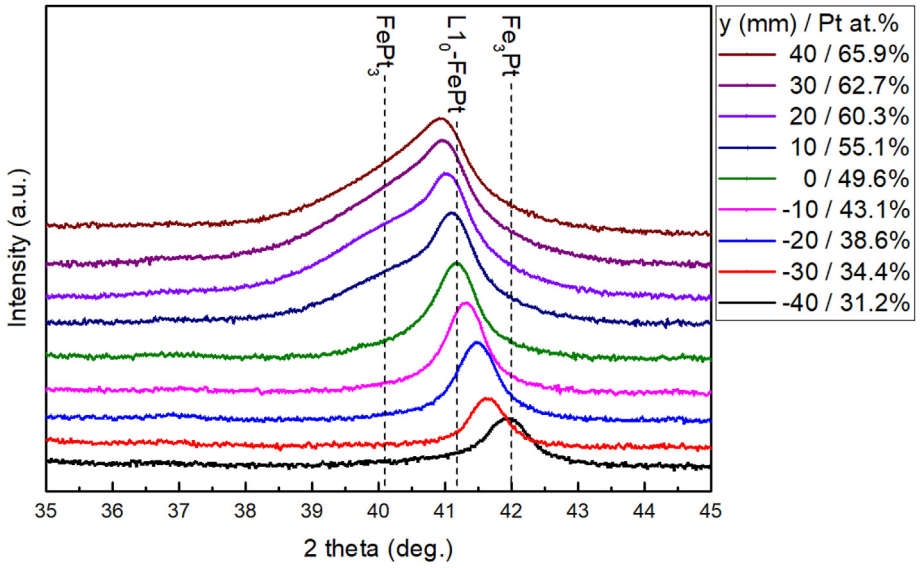

Fig. 9 – Zoom of the XRD patterns of the (111) reflection of Fig. 8. The experimental data is overlaid with dashed lines indicating the position of the (111) peak of chemically ordered $L1_2$-$FePt_3$, $L1_0$-FePt and $L1_2$-Fe_3Pt.

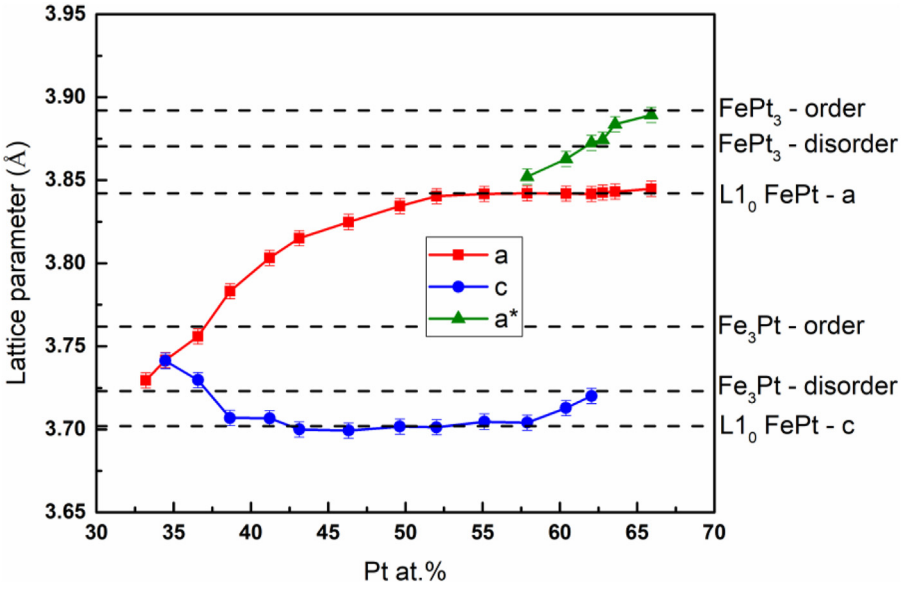

Fig. 10 – The *a* and *c* lattice parameters, estimated according to the position of the (200) and (001) peaks, respectively, plotted as a function of Pt content. The a* lattice parameters are estimated according to the position of the lowest angle peak at the Pt-rich end of the film, which corresponds to the (100) peak of the Pt-rich phase. The dashed lines indicate the lattice parameters of $L1_0$-FePt (#03-065-9121), chemically ordered Fe_3Pt (#04-001-3171), chemically disordered Fe_3Pt (#01-071-8366), chemically ordered $FePt_3$ (#04-017-4976) and chemically disordered $FePt_3$(#04-001-8464).

700 °C. However, significant values of coercivity are maintained at higher Pt content in the present study. A difference in the kinetics of phase ordering in both studies, which could account for the difference in magnetic behaviour, may be explained by the fact that in our case the as-deposited film is an alloy, while in the other it is a wedged multilayer stack, requiring interdiffusion of Fe and Pt layers during the annealing process.

It is important to remark here that the time of acquisition of a 2D set of MOKE loops (on average 323 loops) was approximately 3 h. This is orders of magnitude shorter than the time that would be needed to measure hysteresis loops using a superconducting coil-based magnetometer. Besides, the geometry of the MOKE system allows us to scan over the surface of an intact wafer, while the use of a magnetometer requires the sample to be diced into small pieces with a maximum surface area typically limited to less than 5× 5 mm^2. Nevertheless, the MOKE technique has a number of limitations. It doesn't measure magnetization but rather a rotation of polarized light which is proportional to magnetization. MOKE measurements probe only the properties at the sample surface, to a depth of a few tens of nm, and are thus

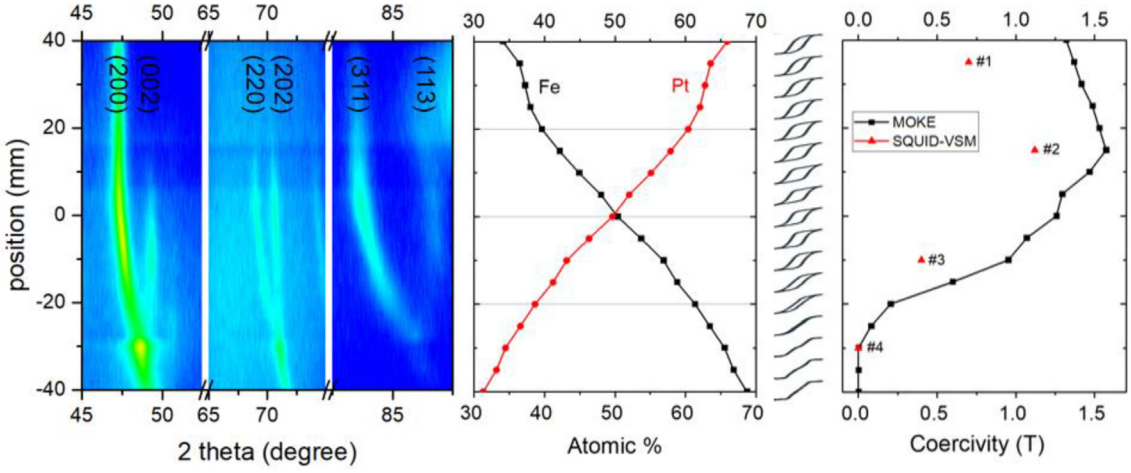

Fig. 11 – 2D Select sections of XRD patterns together with the film composition from EDX, MOKE loops and coercivity values (black symbols), plotted as a function of position along a vertical section of the film annealed at 600 °C for 30 min. Coercivity values estimated from SQUID-VSM measurements of select samples are overlaid on the MOKE coercivity graph (red symbols). (For interpretation of the references to colour in this figure legend, the reader is referred to the Web version of this article.)

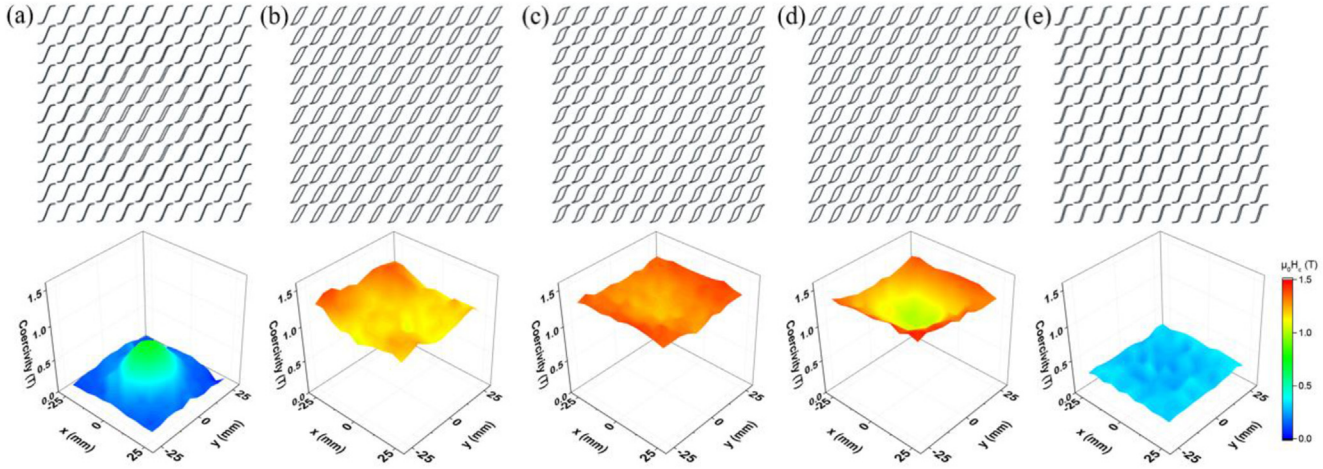

Fig. 12 – Polar MOKE loops and coercivity maps on a 50 × 50 mm^2 region of Fe–Pt films sputtered using targets #4 - #8 and then annealed at 600 °C for 10 min.

not sensitive to any changes in magnetic properties within the volume of the sample. As the technique is based on a measurement of a reflected beam of light, it is not suitable for the characterization of rough surfaces. Thus, scanning MOKE is an ideal approach for high throughput characterization to quickly screen the magnetic behaviour of thin films, and it can be used to select certain samples for more detailed magnetic characterization using traditional techniques such as SQUID-VSM magnetometry. To validate the MOKE measurements, reference out-of-plane SQUID-VSM measurements were made at room temperature on four pieces of the film annealed at 600 °C for 30 min (identified by red boxes in Fig. 7c). Coercivity values from SQUID-VSM measurements are overlaid on the graph of coercivity values measured by MOKE (Fig. 11). The corresponding SQUID-VSM hysteresis loops are shown in the supplementary materials file (S4). The same trend in coercivity as a function of composition is found, though the absolute values are higher for MOKE than for SQUID-VSM (in the samples with highest coercivity, values of 1.13 T and 1.6 T are extracted from SQUID-VSM and MOKE, respectively). The higher values from the MOKE measurements are attributed to viscosity effects [26,27] as a very high field sweep rate (10^6 T/s) occurs during the MOKE measurement while the SQUID-VSM measurement is made under a static field.

3.2. *High throughput preparation and characterization of homogeneous Fe–Pt thin films*

Having demonstrated the use of our scanning MOKE for the high throughput characterization of compositionally graded Fe–Pt films, we will now show another application of it, namely to optimize the fabrication of homogeneous $L1_0$ Fe–Pt films over a large surface area. This is motivated by the desire to be able to integrate such films into parallel processed devices.

A set of films were prepared using targets #4 - #8, which consist of symmetrically positioned pieces of Pt on a base Fe target (Fig. 2). The nominal thickness of the FePt layer was reduced to 50 nm, to suit a specific application (high coercivity coatings of Atomic Force Microscope (AFM) probes to be used as Magnetic Force Microscopy (MFM) probes). Based on the study of the influence of annealing temperature and time on compositionally graded films, and to avoid the risk of diffusion during eventual device fabrication, all films were annealed at 600 °C for 10 min. Figure 12 shows arrays of MOKE loops, together with coercivity maps extracted from these loops, measured from a central section of 50 × 50 mm^2 (this area corresponds to the footprint of the AFM probe holder used in a follow-on study). The films made with the minimum (#4) and maximum (#8) amount of Pt show low values of coercivity, with the former having an inhomogeneous coercivity distribution. All other films show rather homogeneous loops and the highest values of coercivity were measured on the film prepared with target #6. An EDX map of a film

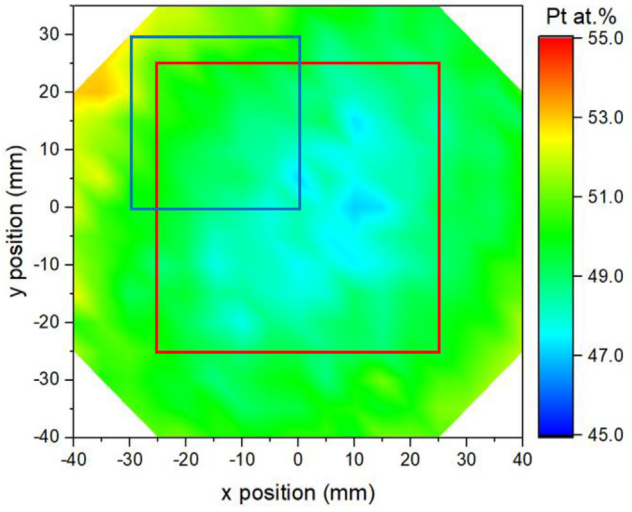

Fig. 13 – 2D EDX map of Pt content measured over a full wafer of a film made using target # 6. The red box indicates the 50 × 50 mm^2 wafer zone probed in Fig. 12, the blue box the 30 × 30 mm^2 region probed in Fig. 14. (For interpretation of the references to colour in this figure legend, the reader is referred to the Web version of this article.)

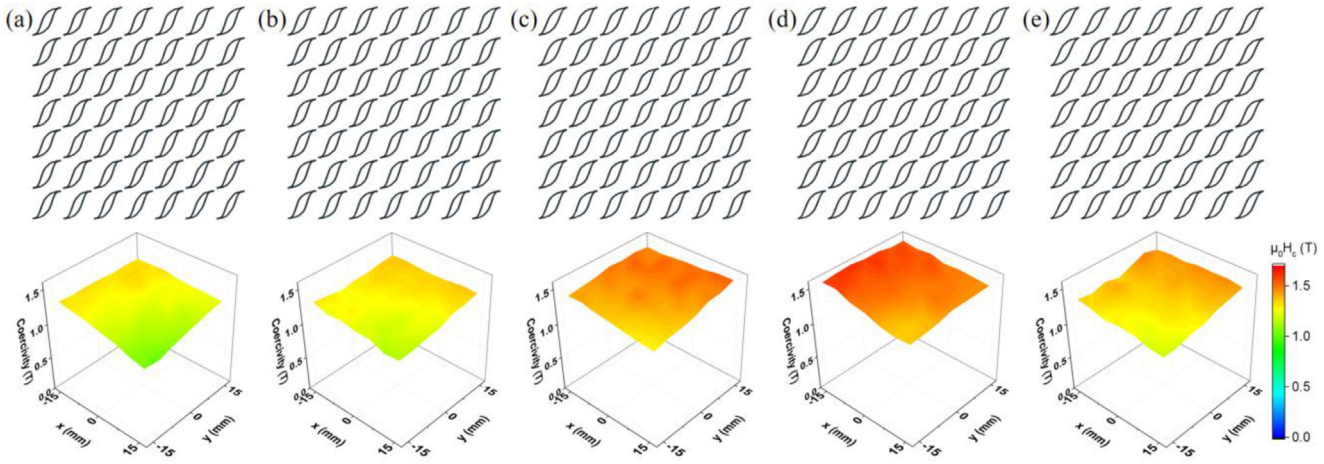

Fig. 14 – Polar MOKE loops and coercivity maps of sections of Fe–Pt films made using target #6, annealed at (a) 500 °C, (b) 550 °C, (c) 600 °C, (d) 650 °C, (e) 700 °C for 10 min.

deposited using this target, shown in Fig. 13, indicates that the composition of the film is rather homogeneous and close to 50 at.% Pt. The red box in Fig. 13 indicates the region probed by scanning MOKE, displayed in Fig. 12. The difference in composition of the samples with maximum coercivity in the graded and homogeneous films may be due to the fact that in the former case we necessarily probe all compositions, while in the latter case we tested five different target geometries which give distinct film compositions. It is possible that with the homogeneous films we are slightly shifted with respect to the optimum composition. Nevertheless, the maximum coercivity values are comparable, so that the offset is not problematic when integrating the films into applications.

The RTA furnace used to anneal the entire wafers of compositionally graded and homogeneous films discussed so far, is not necessarily suitable for the annealing of devices containing Fe–Pt films. This is indeed the case for the first targeted application (MFM probes). For this reason, we studied the use of a tube furnace to anneal homogenous Fe–Pt films and scanning MOKE was also used to re-optimise the annealing temperature of films prepared with target #6. In this case, films were diced roughly into quarters, and different quarters were annealed at different temperatures. Figure 14 shows arrays of MOKE loops, together with coercivity maps extracted from these loops, measured from sections of surface area 30 × 30 mm^2 (an example of one such area is outlined by the blue box in Fig. 13). From this image, we can see that slightly higher values of coercivity can be achieved by increasing the nominal annealing temperature from 600 to 650 °C, while annealing at lower or higher temperatures results in a small drop off in coercivity.

As a final comment, while we did not measure the thickness homogeneity of these films, thanks to the symmetric distribution of Pt pieces on the Fe base, we can expect a radially symmetric thickness distribution. For industrial-scale integration of hard magnetic FePt films into devices on wafers of diameter 50 mm or more, the homogeneity of both thickness and composition, and thus coercivity, can be increased by using bigger targets and increasing the distance between the target and the substrate.

4. Conclusions

A set of high throughput scanning characterization techniques (EDX, high field MOKE and XRD) has been used to study compositionally graded Fe–Pt films of nominal thickness 100 nm. High field MOKE mapping allowed to establish the maximum coercivity values that can be achieved in such Fe–Pt films prepared with the sputtering and annealing systems used in this study (in the case of films annealed at 600 °C for 30 min, coercivity reached ~1.5 T in the composition range 55–60 at.%). The triptych of characterization techniques exploited here holds much potential for the high throughput development of hard magnetic materials through the establishment of massive magnetic and structural data sets. In particular, it may be used to optimize the mixing of different rare earths in known Rare Earth Transition Metal phases (2-14-1, 1–5, 1–12), so as to address the RE-balance problem [28,29]. Beyond this, it could be used to search for new hard magnetic phases in multi-dimensional search spaces. Both challenges will greatly benefit from combining our experimental approach with machine learning approaches, to establish clear correlations between magnetic and structural properties. In a secondary study, the high field MOKE was used to optimize the processing of homogeneous coercive Fe–Pt films, in a step towards their integration into collectively fabricated devices. This demonstrates the tool's potential for use in in-line quality control during device production.

Declaration of Competing Interest

The authors declare that they have no known competing financial interests or personal relationships that could have appeared to influence the work reported in this paper.

Acknowledgements

Y.H. received a grant from the China Scholarship Council (CSC No. 201706150048) to carry out part of his PhD training at Institut Néel. The PhD grant of IdM was jointly financed by the Fondation Nanosciences and the LABEX LANEF (No. ANR-10-LABX-51-01). LANEF is also acknowledged for its support with mutualized infrastructure. This study is partially based on results obtained from the future pioneering program "Development of magnetic material technology for high-efficiency motors (MagHEM), grant number JPNP14015, commissioned by the New Energy and Industrial Technology Development Organization (NEDO), Japan. Funding from the Toyota Motor Corporation is gratefully acknowledged.

Appendix A. Supplementary data

Supplementary data to this article can be found online at https://doi.org/10.1016/j.jmrt.2022.03.055.

REFERENCES

[1] Takeuchi I, Famodu OO, Read JC, Aronova MA, Chang K-S, Craciunescu C, et al. Identification of novel compositions of ferromagnetic shape-memory alloys using composition spreads. Nat Mater 2003;2:180–4.
[2] Green ML, Takeuchi I, Hattrick-Simpers JR. Applications of high throughput (combinatorial) methodologies to electronic, magnetic, optical, and energy-related materials. J Appl Phys 2013;113:231101.
[3] Decker P, Naujoks D, Langenkämper D, Somsen C, Ludwig A. High-throughput structural and functional characterization of the thin film materials system Ni–Co–Al. ACS Comb Sci 2017;19:618–24.
[4] Alexandrakis V, Wallisch W, Hamann S, Varvaro G, Fidler J, Ludwig A. Combinatorial development of Fe–Co–Nb thin film magnetic nanocomposites. ACS Comb Sci 2015;17:698–703.
[5] Ludwig A, Zotov N, Savan A, Groudeva-Zotova S. Investigation of hard magnetic properties in the Fe–Pt system by combinatorial deposition of thin film multilayer libraries. Appl Surf Sci 2006;252:2518–23.
[6] Enokido Y, Hashimoto R, Kitamura T, Suzuki K, Choi KK, Kitamoto Y. High throughput screening method for thin film $R_2Fe_{14}B$ magnet. IEEE Trans Magn 2020;56:1–5.
[7] Kusne AG, Gao TR, Mehta A, Ke LQ, Nguyen MC, Ho KM, et al. On-the-fly machine-learning for high-throughput experiments: search for rare-earth-free permanent magnets. Sci Rep 2014;4:1–7.
[8] Ludwig A. Discovery of new materials using combinatorial synthesis and high-throughput characterization of thin-film materials libraries combined with computational methods. npj Comput. Mater 2019;5:1–7.
[9] Lyubina J, Isnard O, Gutfleisch O, Müller KH, Schultz L. Ordering of nanocrystalline Fe–Pt alloys studied by in situ neutron powder diffraction. J Appl Phys 2006;100:94308.
[10] Ma DG, M Wang Y, Li YH, Umetsu RY, Ou SL, Yubuta K, et al. Structure and properties of nanoporous FePt fabricated by dealloying a melt-spun $Fe_{60}Pt_{20}B_{20}$ alloy and subsequent annealing. J Mater Sci Technol 2020;36:128–33.
[11] C Chi C, Tseng CC, Huang GR, Tsai HJ, Ouyang C, Hsu WK. Carbon encapsulation of ferromagnetic $L1_0$ FePt nanocrystals with an enhanced coercivity from distorted lattices. J Mater Res Technol 2021;13:83–8.
[12] Hsiao Shih-Nan. FePt thin films: fundamentals and applications. Reference Module in Materials Science and Materials Engineering 2016:1–34. https://doi.org/10.1016/b978-0-12-803581-8.02678-3.
[13] Zotov N, Hiergeist R, Savan A, Ludwig A. Effects of annealing time on the structural and magnetic properties of L10 FePt thin films. Thin Solid Films 2010;518:4977–85.
[14] Berry DC, Barmak K. Effect of alloy composition on the thermodynamic and kinetic parameters of the A1 to L10 transformation in FePt, FeNiPt, and FeCuPt films. J Appl Phys 2007;102:24912.
[15] Lu W, Fan JW, Wang YX, Yan B. Magnetic and structural properties of FexPt100-x on MgO(110) substrates. J Mater Sci 2011;46:3835–9.
[16] Cui WB, Varaprasad BSDChS, Takahashi YK, Shiroyama T, Hono K. Microstructure and magnetic properties of FePt-TiC-C granular thin films for perpendicular recording. Solid State Commun 2014;182:17–21.
[17] Wang J, Hata S, Takahashi YK, Sepehri-Amin H, Varaprasad BSDChS, Shiroyama T, et al. Effect of MgO underlayer misorientation on the texture and magnetic property of FePt-C granular film. Acta Mater 2015;91:41–9.
[18] Seki T, Shima T, Takanashi K, Takahashi Y, Matsubara E, Hono K. $L1_0$ ordering of off-stoichiometric FePt (001) thin films at reduced temperature. Appl Phys Lett 2003;82:2461–3.
[19] Lyubina J, Gutfleisch O, Müller KH, Schultz L, Dempsey NM. Nanocrystalline hard magnetic FePt powders. J Appl Phys 2004;95:7474–6.
[20] Shima T, Takanashi K, Takahashi YK, Hono K. Preparation and magnetic properties of highly coercive FePt films. Appl Phys Lett 2002;81:1050–2.
[21] Dias A, Gomez G, Givord D, Bonfim M, Dempsey Nora M. Preparation and characterisation of compositionally graded SmCo films. AIP Adv 2017;7:56227.
[22] Sigurd T, Hamann S, Ludwig A. Modular high-throughput test stand for versatile screening of thin-film materials libraries. Sci Technol Adv Mater 2011;12:54206.
[23] Zambano AJ, Oguchi H, Takeuchi I, Choi Y, Jiang JS, Liu JP, et al. Dependence of exchange coupling interaction on micromagnetic constants in hard/soft magnetic bilayer systems. Phys Rev 2007;75:144429. B.
[24] Laegreid N, Wehner GK. Sputtering yields of metals for Ar+ and Ne+ ions with energies from 50 to 600 ev. J Appl Phys 1961;32:365.
[25] Hsiao SN, Chen SK, Hsu YW, Yuan FT, Huang HW, Chin TS, et al. Magnetic properties and crystallographic structure of Fe3Pt thin films. IEEE Trans Magn 2008;44:3902–5.
[26] Street R, Woolley JC. A study of magnetic viscosity. Proc. Phys. Soc., Sect 1949;62:562. A.
[27] Wohlfarth EP. The coefficient of magnetic viscosity. J Phys F Met Phys 1984;14:L155.
[28] Binnemans K, Jones PT, Van Acker K, Blanpain B, Mishra B, Apelian D. Rare-earth economics: the balance problem. JOM (J Occup Med) 2013;65:846–8.
[29] Jowitt SM, Werner TT, Weng ZH, Mudd GM. Recycling of the rare earth elements. Curr. Opin. Green Sust 2018;13:1–7.